ORIGINAL ARTICLE

Cytotoxic effect of green synthesized silver nanoparticles in MCF7 and MDA-MB-231 human breast cancer cells in vitro

Arindam Bandyopadhyay[1] · Bishnupada Roy[2] · Pallab Shaw[1] · Paritosh Mondal[1] · Maloy Kr. Mondal[2] · Pranesh Chowdhury[2] · Shelley Bhattacharya[1] · Ansuman Chattopadhyay[1]

Abstract

With the incessant rise in the cancer burden worldwide it is a dire need to develop anticancer agents that will offer negligible or no side effects and at the same time will be economically feasible. In this study, we utilized the principle of green chemistry where tyrosine and chitosan were used as reducer and stabilizer respectively to synthesize biocompatible silver nanoparticles. They were characterized by ultraviolet–visible spectroscopy, transmission electron microscopy and dynamic light scattering technique and found to be spherical with average diameter of 13–22 nm. Their toxicity was evaluated in MCF7 and MDA-MB-231 human breast cancer cell lines. MTT assay revealed excellent cytotoxic effect with IC_{50} values as low as 6.4 and 6.56 ppb respectively after 48 h of treatment. Intriguingly, they showed minimum toxicity in normal human peripheral blood lymphocytes at these effective concentrations. Cytomorphological alteration, ROS generation (DCFDA analysis) and nuclear fragmentation (Hoechst staining) were pronounced in both cancer cell lines following treatment. These nanoparticles also promoted expression and nuclear translocation of Nrf2 as an antioxidant response which was revealed by Western blot and immunofluorescence studies respectively. 'Apoptosis assay' confirmed the presence of apoptosis and 'Caspase-8 activity assay' revealed absence of the extrinsic apoptosis pathway. Western blot data (upregulation of p21, Bax/Bcl2 ratio, Caspase-9, Caspase-3 and cleaved PARP1) established the occurrence of intrinsic apoptosis pathway following cell cycle arrest. To conclude, the green synthesized silver nanoparticles are cytotoxic to cancer cells and can be considered as effective and safe cytotoxic agents in breast cancer therapeutics.

Keywords Silver nanoparticles · Chitosan · Breast cancer · Intrinsic apoptosis

Introduction

Silver nanoparticles (AgNPs), although utilized mostly for their broad-spectrum antimicrobial activity, have been extensively used in several diseases over the past few years due to their unique physicochemical properties [17, 19, 46]. Cytotoxic efficacy of AgNPs produced via different routes has also been reported in different types of cancer cells including breast cancer, cervical cancer, oral cancer, skin melanoma and several other cancer cell lines [3, 5, 6, 14, 16]. Chemical or photochemical methods employed to synthesize AgNPs

are potent threat to the environment that limits their medical application. Contrastingly, nanoparticles synthesized using biological methods which employs fungi, algae, different plant parts or biomolecules like amino acids, starch, vitamins etc. are considered as 'green' nanoparticles as far as their eco-safety and biocompatibility are concerned [7, 15, 46]. So, it is of prime importance that besides being effectively cytotoxic to cancer cells synthesized AgNPs will be environmentally safe, economically cheap and at the same time safe to noncancerous cells.

Although AgNPs synthesized utilizing the reducing property of several phytochemicals get maximum attention in terms of medicinal use [5, 14], other bioorganic materials like chitosan are also attractive options in this regard. Chitosan is a naturally occurring polysachharide which is biodegradable, biocompatible and non-toxic. It is obtained by deacetylation of chitin, abundantly found in crustacean shells and fungal cell walls. Moreover, it also enhances

✉ Ansuman Chattopadhyay
  chansuman1@gmail.com

1 Department of Zoology, Visva-Bharati, Santiniketan, West Bengal 731235, India

2 Department of Chemistry, Visva-Bharati, Santiniketan, West Bengal 731235, India

cellular penetration that promotes transport of NPs inside cells which is another advantage of this chemical. In this experiment, we prepared chitosan-functionalized AgNPs following reduction of silver nitrate by amino acid tyrosine and further stabilization by chitosan [12, 34].

Two different types of breast cancer cell lines were considered to check the cytotoxic potential of these chitosan-functionalized AgNPs (S_1). MCF7 and MDA-MB-231 human breast cancer cell lines differ from each other in the nature of their response to hormone therapies. MCF7 is having both estrogen receptor (ER) and progesterone receptor (PR) but lacks human epidermal growth factor receptor 2 (HER2) [13]. In contrast, MDA-MB-231 is a triple-negative breast cancer (TNBC) cell line which lacks all three receptors viz. ER, PR and HER2 and thus is incurable by hormone therapy [2]. Cytotoxic effect of these NPs was compared with that of Mitomycin-C, a well-known anticancer drug [1]. Their innocuous nature was also investigated in normal cells- human peripheral blood lymphocytes (HPBLs), in vitro.

Materials and methods

Materials

Silver nitrate (Merck, India), chitosan (Practical grade, 75% deacetylated, Aldrich, Germany) and L-tyrosine hydrochloride (Sigma life sciences, USA) were used as received. Dulbecco's Modified Eagle's Medium (DMEM) and Roswell Park Memorial Institute (RPMI)-1640 culture media, penicillin–streptomycin antibiotic solution, phytohaemagglutinin (PHA), foetal bovine serum (FBS), radioimmunoprecipitation assay (RIPA) buffer, MTT (3-[4,5-dimethylthiazol-2-yl]-2,5-diphenyltetrazolium bromide) and skim milk were procured from Himedia Laboratories, India; BCIP/NBT (5-bromo-4-chloro-3-indolyl phosphate/nitro blue tetrazolium), 2′,7′- dichlorofluorescein diacetate (DCFDA) and DMSO (dimethyl sulfoxide) were purchased from Merck, India; Mitomycin-C (Kyowa Hakko Kogyo Ltd., Japan), heparin, trypan blue and triton X-100 were procured from Sisco Research Laboratories, India; histopaque, anti-human primary antibodies (Sigma-Aldrich, USA), ALP-linked goat anti-rabbit (Abcam, UK) and anti-mouse (Genei, India) secondary antibodies were used as received. Trigonelline hydrochloride was purchased from Santa Cruz Biotechnology, USA. Caspase-8 Assay Kit, goat anti-rabbit FITC-conjugated secondary antibody, DAPI (4′, 6-diamidino-2-phenylindole), bisbenzimide (Hoechst 33,342) and bovine serum albumin (BSA) were procured from Sigma-Aldrich, USA. Cell-APOPercentage Apoptosis Assay kit was purchased from Biocolor, UK. Double distilled water was used throughout.

Instrumentation

Branson 1510 sonicator was used to obtain an ultrasound frequency of 40 kHz. UV–VIS spectrophotometer (Shimadzu, Model UV-PC) was used for the detection of surface plasmon resonance of the samples. The sample for TEM was prepared using carbon-coated copper grids in a JEOL TEM-2010 instrument. Size distribution (DLS) of the particles was carried out using a Malvern Zetasizer Ver.6.34 instrument.

Synthesis of silver nanoparticles

The preparation of chitosan-functionalized AgNPs (S_1) was done following the protocol reported by Roy et al. [41]. A very small volume of tyrosine solution (10^{-3} M) was added to the silver nitrate solution (10^{-3} M) at the volume ratio of 20:1 and irradiated in a microwave oven for 1 min. Then a chitosan solution (2.5% chitosan) was added maintaining the volume ratio of 20:1:2. The whole mixture was subjected to sonication. Ultraviolet–visible (UV–Vis) spectral analysis was carried out to monitor the reaction by checking the SPR (surface plasma resonance) behavior of AgNps. The AgNps were purified by ultracentrifugation and then re-dispersed in 1% acetic acid solution according to the desired concentration. Finally the sample was stored in a cool dry place to check the stability. The color of sample was golden yellow and it was fairly stable (Fig. 1a). Solution of all chemicals other than silver nitrate used to synthesize these NPs was considered as suspension media of AgNPs (S_2).

Cell viability assay in MCF7 and MDA-MB-231

Human breast cancer cell line MCF7 and MDA-MB-231 were procured from the National Centre for Cell Science (Pune, India). Cells were cultured in complete DMEM media (with 10% FBS and 1% penicillin–streptomycin solution) and incubated at 37 °C in presence 5% humid CO_2 (Thermo Fisher Scientific, USA).

Cells were further seeded at a density of 2×10^4 cells mL^{-1} in a 96 well plate and after 24 h, treated with different concentrations of S_1 (2.66, 5.32 and 8 ppb) and their corresponding equal volume of S_2 for another 48 h. Untreated control cells and Mitomycin-C (50 μM)-treated cells were kept as negative and positive control respectively. To check the cell viability after 48 h of treatment cells were treated with 5 mg mL^{-1} MTT solution for 4 h. Blue-purple formazan crystals are formed by the living cells following reduction of yellow tetrazolium salt (MTT) by mitochondrial dehydrogenase. The crystals were dissolved in the DMSO after discarding culture media and the optical density (OD)
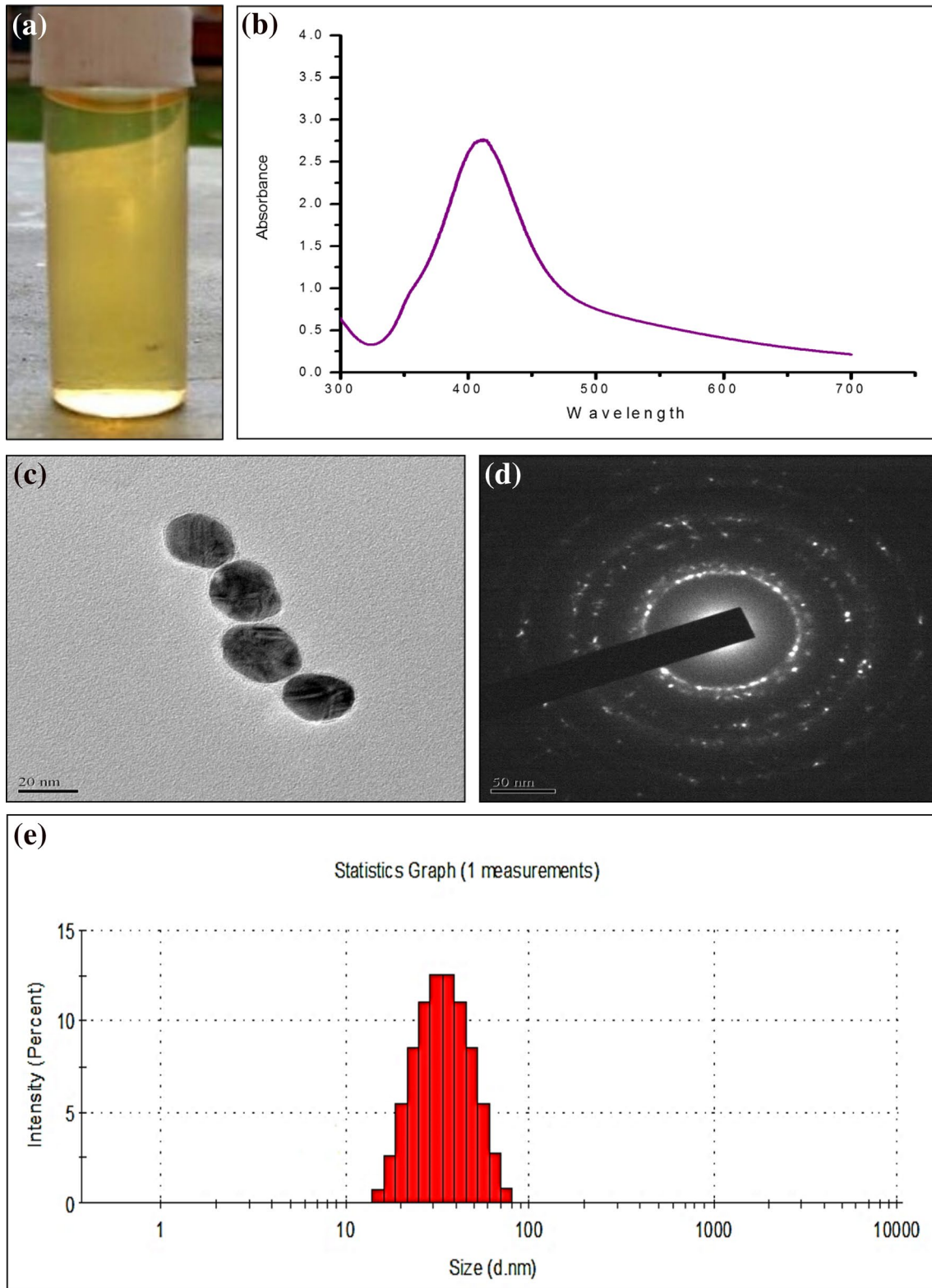
Fig. 1 Synthesis and characterization of chitosan-functionalized silver nanoparticles (S₁). Synthesized S₁ (**a**); their UV–Visible spectrum (**b**); transmission electron microscopic (TEM) image (**c**); selected area electron diffraction (SAED) image (**d**) and dynamic light scattering (DLS) pattern (**e**)

was measured at 595 nm in iMark™ Microplate Absorbance Reader (BIO-RAD, USA). OD of the untreated control group was considered equivalent to 100% living cells and cell survival (%) of treated groups was calculated from respective OD values. All experiments were performed in triplicate on three separate occasions and data are presented as mean ± standard error of means (SEM).

Cell viability assay in human peripheral blood lymphocytes, in vitro

Fresh human blood was collected for isolation of lymphocytes. The donors were non-alcoholic, non-smoker male of 23–27 years of age group. The collection was done by experts under the supervision of doctors and with the prior consent of the donors. The experiment was executed following the guidelines of Indian Council of Medical Research, India (Ethical Guidelines for Biomedical Research on Human Subjects) with prior approval of "Institutional Ethics Committee for Human Research" of Visva-Bharati University, India.

The isolation of lymphocytes was done following the method of Bøyum [9] with minor modifications as described by Bandyopadhyay et al. [4]. In brief, HPBLs were isolated following density gradient centrifugation using histopaque and cultured in complete RPMI-1640 media (with 10% FBS and 1% penicillin–streptomycin solution) at a density of 2×10^4 cells mL^{-1} following PHA-stimulation and incubated at 37 °C (Thermo Fisher Scientific, USA). After 24 h of culture, HPBLS were treated with IC$_{50}$ concentrations of S$_1$ in cancer cells for 48 h and viability was checked using MTT assay as described in the previous section.

Cytomorphological evaluation

The microscopic study was performed to see the alteration in normal cellular morphology in cancer cells following incubation with the synthesized NPs. Both MCF7 and MDA-MB-231 cells were treated with respective half-maximal inhibitory concentrations (IC$_{50}$) of S$_1$ for 48 h and studied using an inverted phase-contrast microscope (Dewinter, Italy) at a magnification of 200×.

Detection of reactive oxygen species

The presence of reactive oxygen species (ROS) in both the breast cancer cell lines was detected following 48 h-exposure to respective 1/3rd IC$_{50}$ concentrations of S$_1$ through DCFDA analysis. As it is known that NPs interfere with this assay [28], measures were taken to nullify the same. Culture media of both control and treatment groups were removed and cells were collected in PBS following centrifugation at 2000 rpm for 5 min. In this way, AgNPs were completely eliminated from the system before proceeding to conduct the assay. Cells were further incubated with 10 mM DCFDA for 5 min and visualized through a fluorescent microscope (Dewinter, Italy). Fluorescent DCF was detected which is generated by ROS-mediated oxidation of deacetylated DCFDA.

Immunofluorescence assay of Nrf2

Nuclear localization of Nrf2 is a crucial indicator of the presence of oxidative stress. This assay was performed to evaluate the same in breast cancer cells following S$_1$ treatment. The assay followed the method described by Mukherjee et al. [35]. In brief, breast cancer cells were cultured on coverslips and treated with 1/3rd IC$_{50}$ of S$_1$ for 48 h. A 48 h co-treatment of NPs and trigonelline (Nrf2-inhibitor, 1 μM) was also applied. After careful washing with phosphate-buffered saline (PBS), cells were fixed in chilled methanol, permeabilized with triton X-100 and blocked using BSA. Cells were subsequently incubated with Nrf2 antibody and FITC-conjugated secondary antibody followed by counterstaining with a nuclear stain DAPI. Finally, cells were mounted on clean glass slides with mounting medium and images were captured using a confocal fluorescent microscope (Leica TCS-SP8).

Detection of nuclear fragmentation

Nuclear fragmentation in cancer cells was detected by Hoechst staining. Cells were grown on coverslip and treated with 1/3rd IC$_{50}$ of S$_1$ for 48 h. Following that, cells were washed with PBS and fixed using 4% paraformaldehyde. Cells were again washed using PBS and subsequently incubated with Hoechst (5 μg/mL) for 10 min at 37 °C. After that, cells were mounted on glass slides and visualized using an inverted fluorescent microscope (Leica).

Apoptosis assay

To decipher the route of cell death triggered by the NPs this assay was performed. For this, we used the Cell-APOPercentage Apoptosis Assay kit (Biocolor, UK) and followed their protocol. Briefly, cancer cells were treated with respective 1/3rd IC$_{50}$ of S$_1$ for different time points viz. 2 h, 24 h, and 48 h to monitor the temporal effect of NPs in these cell lines. Cells were incubated with a dye just 30 min prior to completion of each experiment to stain only apoptosis-induced cells and apoptotic bodies. The microscopic study was performed at 200× using an inverted phase-contrast microscope (Dewinter, Italy) and images were captured using Bio-Wizard software. Cells were further trypsin-digested and incubated with a dye releasing agent. The concentration of dye was measured colorimetrically at 550 nm.

Caspase-8 activity assay

Activity of Caspase-8, an initiator caspase of extrinsic apoptosis pathway, was evaluated in the cancer cells following the manufacturer's (Caspase-8 Assay Kit, Sigma-Aldrich, USA) protocol. In brief, cells were collected after 2 h, 24 h, and 48 h of treatment with respective 1/3rd IC_{50} concentration of S_1. They were lysed in chilled RIPA buffer and supernatants were collected following centrifugation at 12,000 rpm, 4 °C for 20 min. Supernatants were further incubated with Acetyl-Ile-Glu-Thr-Asp-*p*-nitroaniline (Ac-IETD-pNA), a substrate of Caspase-8. Active Caspase-8 cleaves the bond between Asp and *p*-nitroaniline releasing chromophore pNA in the solution. Presence of this chromophore was detected at 405 nm in both control and treated samples (iMark™ Microplate Absorbance Reader, BIO-RAD, USA).

Western blot analysis

Western blot analysis was performed as described by Banerjee et al. [5]. In brief, cancer cells were treated with respective 1/3rd IC_{50} of S_1 for 2 h, 24 h, and 48 h, collected and lysed in chilled RIPA buffer. To detect the Nrf2 expression pattern, only 2 h and 48 h exposures were considered as initial and end point detection. In all cases, the amount of total protein in cell lysate after centrifugation was quantified following the Lowry et al. [30]. Sodium dodecyl sulfate–polyacrylamide gel electrophoresis (SDS-PAGE) was performed to check the level of individual protein of interest in untreated control and treated groups. Proteins were blotted onto polyvinylidene fluoride (PVDF) membranes from the gel. Blots were incubated with respective primary antibodies (Nrf2, p53, p21, Bcl2, Bax, Caspase-9, Caspase-3, PARP1 and β-actin) and subsequently with corresponding secondary antibodies. ALP-linked goat anti-rabbit secondary antibodies were used for Nrf2, Bcl2, Caspase-9, Caspase-3 and PARP1. For p53, p21, Bax, and β-actin ALP-linked anti-mouse secondary antibodies were used. The bands were developed after incubation with BCIP/NBT.

All the biological experiments throughout this study were conducted in triplicates (n = 3).

Results and discussion

Green synthesis and characterization of silver nanoparticles

Chitosan-functionalized AgNPs (S_1) were prepared using the principles of green chemistry where not only tyrosine and chitosan are biodegradable but also the reaction medium is environmentally benign. Bio-molecule tyrosine (enol form) reduced the silver ion through one electron transfer process and itself oxidized to its keto form. Thus tyrosine acted as a reducing agent. The additive chitosan stabilized the AgNPs through the well-known corona type core–shell structure [41].

UV–Vis spectroscopy revealed surface plasmon absorption of S_1 at around 410 nm (Fig. 1b) which fits within the range of characteristic peak exhibited by AgNPs [24]. The peak is the consequence of resonance oscillation of conduction electrons, which results in the formation of a dipole in the material due to absorption of electromagnetic waves.

Transmission electron microscopic (TEM) image of S_1 was recorded after drop casting metal nanoparticle samples on the carbon-coated copper grid (Fig. 1c). It is evident from the image that the nanoparticles were mostly spherical in shape (isotropic i.e. low aspect ratio) with average diameter of 13–22 nm. Presence of well-known lattice fringe in the TEM image and illuminated circular dotted rings in SAED (selected area electron diffraction) pattern (Fig. 1d) suggest the polycrystalline nature with face-centered cubic geometry of the sample [27].

The dynamic light scattering (DLS) study revealed that the average size distribution of AgNPs (Fig. 1e) at around 30 nm. The small difference in size between DLS and TEM is probably due to the presence of hydrophilic polymer around these NPs. The protonated amine group of chitosan attracts the negative dipole of water molecule causing considerable change in hydrodynamic size, which is greater than the NPs themselves.

Silver nanoparticles reduced cancer cell viability in a dose-dependent manner, altered cellular morphology and appeared less cytotoxic to normal HPBLs

Both MCF7 and MDA-MB-231 were exposed to different concentrations of S_1 along with respective equal volume of suspension media viz. S_2. Cells were also treated with Mitomycin-C (50 μM) as a positive control which showed around 50% cell survival in both breast cancer cell lines. S_1 reduced cell survival of both MCF7 and MDA-MB-231 in a dose-dependent manner (Fig. 2a, b) and half-maximal inhibitory concentrations (IC_{50}) were found to be 6.4 and 6.56 ppb respectively after 48 h of treatment. Interestingly, when the cells were treated with respective equal volume of suspension media (without NPs), 100% cell survival was recorded demonstrating the role of S_1 in cancer cell death. At these concentrations, S_1 also caused significant cytomorphological alterations in cancer cells which were found to be shrunk, clumped and with less or no lamellar expansions as compared to control (Fig. 2c, d).

When the effect of S_1 was investigated in HPBLs in vitro it was found that these NPs did not reduce the survival of normal cells at effective anticancer dose (48 h-IC_{50}) which
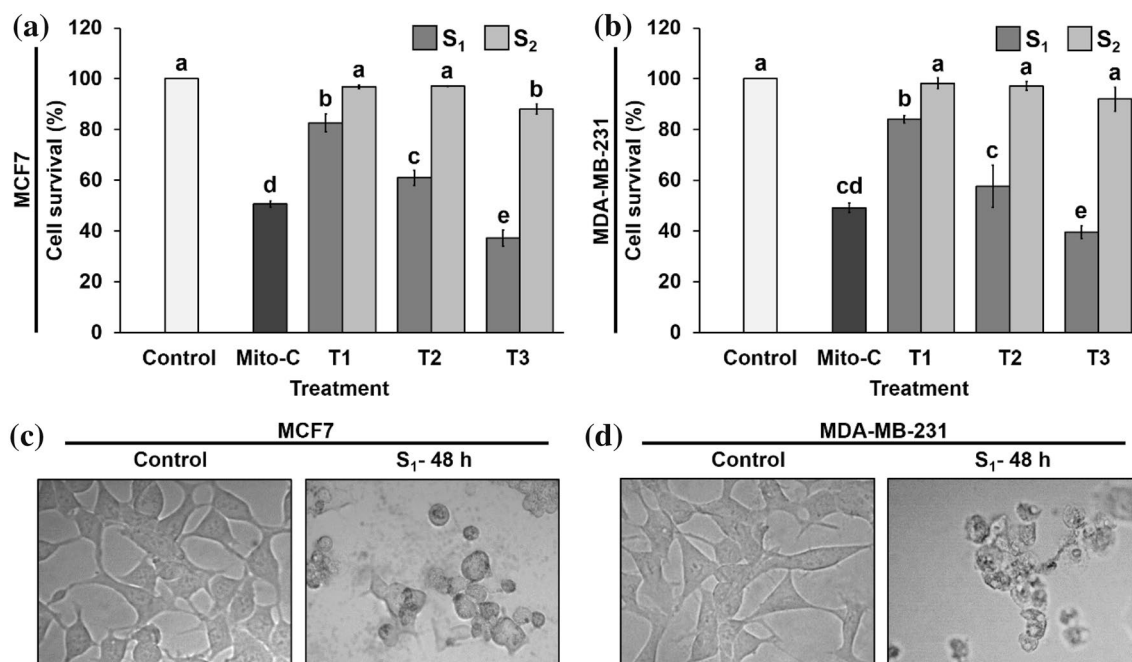
Fig. 2 Evaluation of cell survival and morphology. Survival (%) of MCF7 (**a**) and MDA-MB-231 (**b**) human breast cancer cells upon exposure to different concentrations of chitosan-functionalized silver nanoparticles (S_1) and their respective suspension media (S_2) for 48 h. Treatments T1, T2, and T3 represent 2.66, 5.32 and 8 ppb of S_1 and their corresponding equal volume of S_2 respectively. Mitomycin-C (Mito-C)-treated (50 μM) cells were taken as positive control. Tests were performed in triplicate and the graphs represent

their mean ± SEM value. Statistical analysis was done using one-way ANOVA following Tukey method in Minitab 17 software. Means that do not share a letter are significantly different. Significance level α = 0.05. Figure **c** and **d** represent photomicrographs of MCF7 and MDA-MB-231 respectively without treatment (Control) and after 48 h-exposure to the IC_{50} concentrations of S_1 to detect alterations in normal cellular structure (microscopic magnification 200×)

projected them as safer alternative and prompted us to explore the detail mechanism involved in cancer cell death caused by them.

Promotion of ROS level, subsequent expression and nuclear translocation of Nrf2

S_1 successfully induced significant ROS generation in both MCF7 (Fig. 3a) and MDA-MB-231 (Fig. 3b) as evidenced by presence of bright green fluorescence in treated cells. Besides that, a significant elevation in the Nrf2 expression (1.3–1.6 fold increase) was noticeable after 48 h of treatment (Fig. 3c, e). The immunofluorescence data also revealed a marked increase in the nuclear Nrf2 level in both the cell lines at this time point (Fig. 3d, f merged images). Interestingly, co-incubation with NPs and Nrf2-inhibitor trigonelline for 48 h did not alter the Nrf2 status inside the nuclei of both cell lines as compared to control. It is a well-established fact that AgNPs generate intracellular reactive oxygen species (ROS) [32, 45]. Intracellular oxidative stress is a potent promoter of the expression and nuclear translocation of Nrf2, a transcription factor, that plays a crucial role to protect cells from oxidative damages by activating a myriad of genes involved in antioxidant

defense system and cellular protection [31, 36]. In our experiment, increased ROS level indicated that the NPs induced oxidative stress in breast cancer cells that tried to combat the oxidative damage by employing the key stress regulator Nrf2. These findings prompted us to explore further the mechanism of cell death triggered by these NPs.

Nuclear fragmentation and activation of PARP1

Following S_1 exposure, profound nuclear fragmentation was detected by Hoechst staining in both MCF7 (Fig. 4a) and MDA-MB-231 (Fig. 4b). It is an indication of chromatin condensation and DNA fragmentation [10]. Whereas, control cells exhibited properly shaped intact nuclei. This finding can be well corroborated with the level of ROS in S_1-treated cells as it is a well-established fact that ROS induces DNA damage [33]. In this situation, poly(ADP-ribose) polymerase-1 (PARP-1) plays an important role to repair DNA and maintain genomic integrity [11, 38]. In this experiment, PARP1 was also found to be overexpressed following 48 h of treatment in both cell lines indicating cellular response to cope up oxidative DNA damage (Fig. 5a, b).
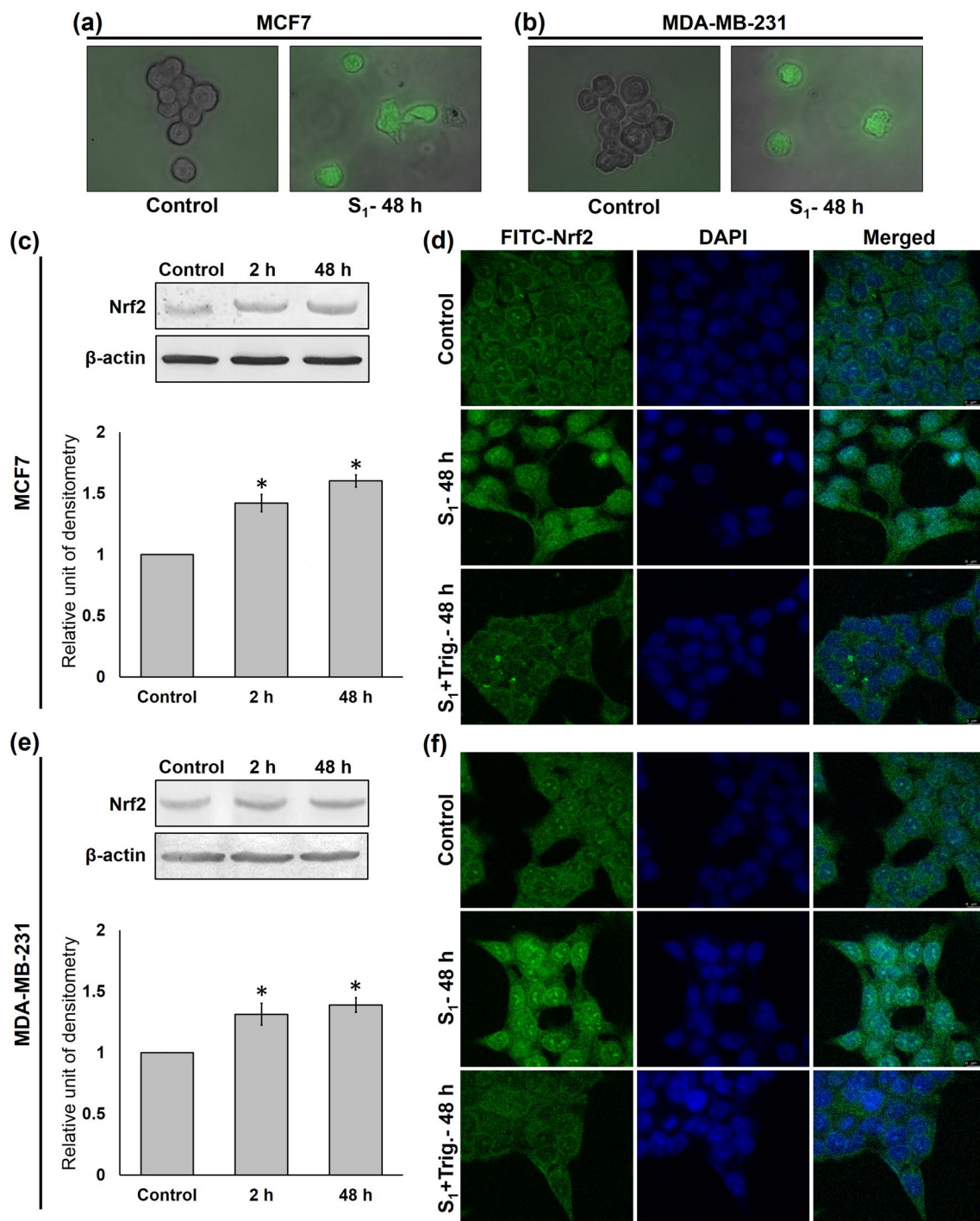
Fig. 3 Detection of reactive oxygen species (ROS) and evaluation of expression and nuclear localization of Nrf2. ROS was determined through DCFDA analysis in MCF7 (**a**) and MDA-MB-231 (**b**) following 48 h-exposure to respective 1/3rd IC$_{50}$ of chitosan-functionalized silver nanoparticles (S$_1$). Bright green fluorescence indicates ROS which is shown in merged images (bright-field image + fluorescence image) at a magnification of 200×. Protein expression of Nrf2 and its relative densitometries after 2 h and 48 h incubation with 1/3rd IC$_{50}$ of S$_1$ in MCF7 (**c**) and MDA-MB-231 (**e**). Relative densitometry was performed after normalizing the data taking β-actin as an inter-

nal control. The ImageJ 1.52a software was used in this purpose and relative densitometry of the data from three independent experiments are expressed as the mean ± SEM (*significantly different from control $p < 0.05$). Figure **d** and **f** represent photomicrographs taken using a confocal fluorescent microscope (Leica TCS-SP8) showing nuclear translocation of Nrf2 in the untreated control, after 48 h treatment of 1/3rd IC$_{50}$ of S$_1$ and after a co-treatment of S$_1$ and trigonelline (Trig; an Nrf2-inhibitor, 1 μM) for 48 h in MCF7 and MDA-MB-231 respectively. Scale bar = 10 μm
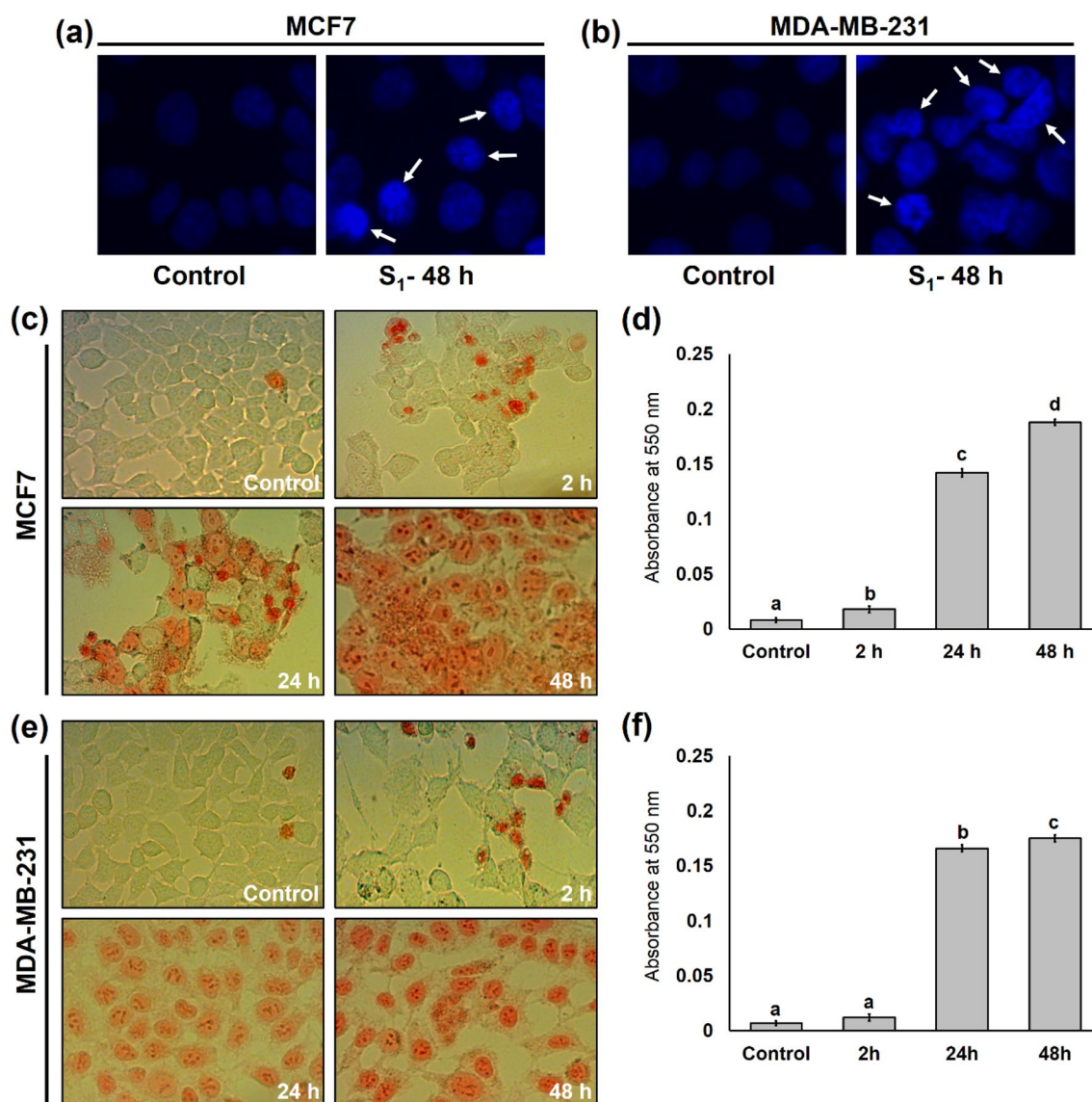
Fig. 4 Detection of nuclear fragmentation and apoptosis induction. Nuclear fragmentation (indicated by arrows) in both MCF7 (**a**) and MDA-MB-231 (**b**) was analyzed through Hoechst staining following 48 h-exposure to respective 1/3rd IC_{50} concentrations of chitosan-functionalized silver nanoparticles (S_1) (microscopic magnification 400×). Apoptosis induction was detected microscopically in MCF7 (**c**) and MDA-MB-231 (**e**) at 200× using an inverted phase-contrast microscope (Dewinter, Italy) and was quantified colorimetrically at 550 nm (**d** and **f**). The data from three independent experiments are expressed as the mean ± SEM. Statistical analysis was done using one-way ANOVA following Tukey method in Minitab 17 software. Means that do not bear the same letter are significantly different. Significance level $\alpha = 0.05$

Apoptosis as the mode of cell death

Both microscopic and colorimetric data evidenced the induction of apoptosis just after the 2 h of NP-exposure in both the cell lines which simultaneously increased manifold after 24 h and 48 h of treatments (Fig. 4c, f). The cells that retained the red dye were undergoing apoptosis and their number increased 23–25 fold in both cell lines after 48 h of S_1 treatment. This assay clearly depicted that the breast cancer cells upon exposures to S_1 underwent apoptosis as a route of cell death and did not follow the necrotic pathway. And apoptosis is advantageous over necrosis as the latter induces a systemic inflammatory response following cell demises that can cause bodily harms [42].

Execution of apoptosis via intrinsic pathway following cell cycle arrest

Negative result of Caspase-8 activity assay after S_1-exposure revealed that both the breast cancer cell lines underwent
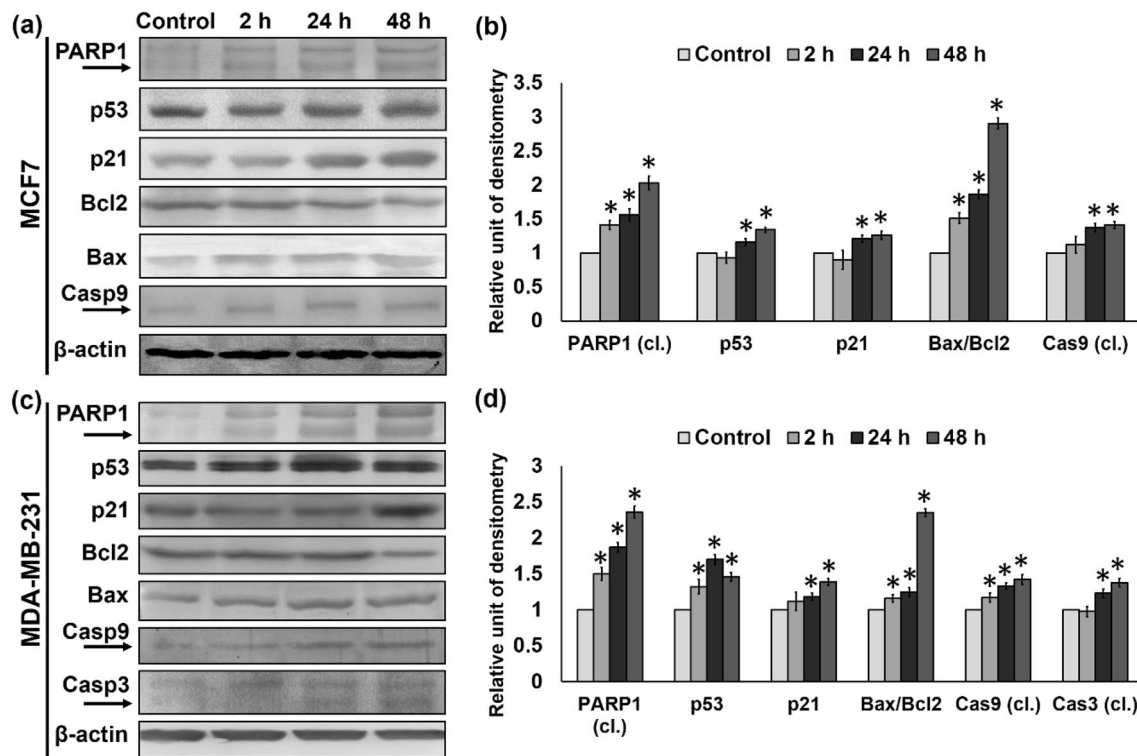
Fig. 5 Western blot analysis after exposure to 1/3rd IC_{50} concentrations of chitosan-functionalized silver nanoparticles (S_1) for 2 h, 24 h, and 48 h. Expression patterns of PARP1, p53, p21, Bcl2, Bax, cleaved Caspase-9 (Casp9, arrow-indicated), and β-actin in MCF7 were shown in blots **a**. In case of MDA-MB-231, blots representing cleaved Caspase-3 (Cas3, arrow-indicated) are also shown **c**. Arrows in the PARP1 indicate its cleaved form. Protein expression was quantified using relative densitometry where β-actin was used as an internal control. The ImageJ 1.52a software was used in this purpose and relative densitometry of the data from three independent experiments are expressed as the mean ± SEM (*significantly different from control $p < 0.05$). Graphs show Bax/Bcl2 expression ratio along with the expression of other mentioned proteins in MCF7 (**b**) and MDA-MB-231 (**d**). *cl.* cleaved

apoptosis through Caspase-8-independent pathway. Presence of Caspase-8 activity is the hallmark of the extrinsic apoptosis pathway and its absence prompted us to investigate the apoptosis in the light of the intrinsic pathway (Fig. 5). Normal cell cycle progresses through G1, S, G2 and mitosis and it can be compromised under stress and in this condition the p53-p21 pathway plays an important role to pause the cell cycle at the initial G1 phase [39]. Generally, p21 expression is positively regulated with the level of p53 but reports are there on p53-independent upregulation of p21 [21, 22, 40]. In the case of MCF7, p21 expression was found to be positively regulated by p53 but aberrant expression of the latter in MDA-MB-231, which is a p53-mutant cell type, indicated p53-independent p21 expression in this cell line. This finding can also be correlated with previous reports [5, 18, 23]. Level of both p53 and p21 in MCF7 and p21 in MDA-MB-231 spiked after 24 h of treatment. Besides arresting cell cycle progression at G1/S transition, p21 also blocks cells at G2 phase by inhibiting cyclin dependent kinases [25]. Depending on p21 expressional profile it can be strongly suggested that S_1 inhibited cell cycle progression in both of these cell lines. Anti-apoptotic Bcl2 and

pro-apoptotic Bax are two important proteins involved in the regulation of the intrinsic apoptosis pathway. In both the cell lines, Bcl2 level dropped maximally after 48 h of S_1-exposure, whereas highest level of Bax was detected at the same time point. Simultaneously, Bax/Bcl2 ratio was found upregulated even after 2 h of treatment and it successively increased following 24 h and 48 h exposure (2–3 fold increase after 48 h) which is an important marker for the presence of intrinsic apoptosis. Bax form pores on the outer membrane of mitochondria causing the release of some apoptotic mediators that inevitably activate Caspase-9 which in turn activates Caspase-3 [37, 47]. Caspases are proteases which play the central role to make cells committed to die through apoptosis. The process is progressed through either the mitochondria-mediated Caspase-9-dependent intrinsic pathway or the death-ligand-dependent Caspase-8-mediated extrinsic pathway [8, 20]. Both of these caspases are 'initiator' caspases which, upon activation by their cleavage, trigger a downstream cascade leading to activation of 'effector' caspases. Caspase-3 is one such effector caspases which once activated cleaves a broad spectrum of cellular targets leading to cell demise [43]. This role is played by

Fig. 6 Cellular response of MCF7 and MDA-MB-231 human breast cancer cell lines to chitosan-functionalized silver nanoparticles
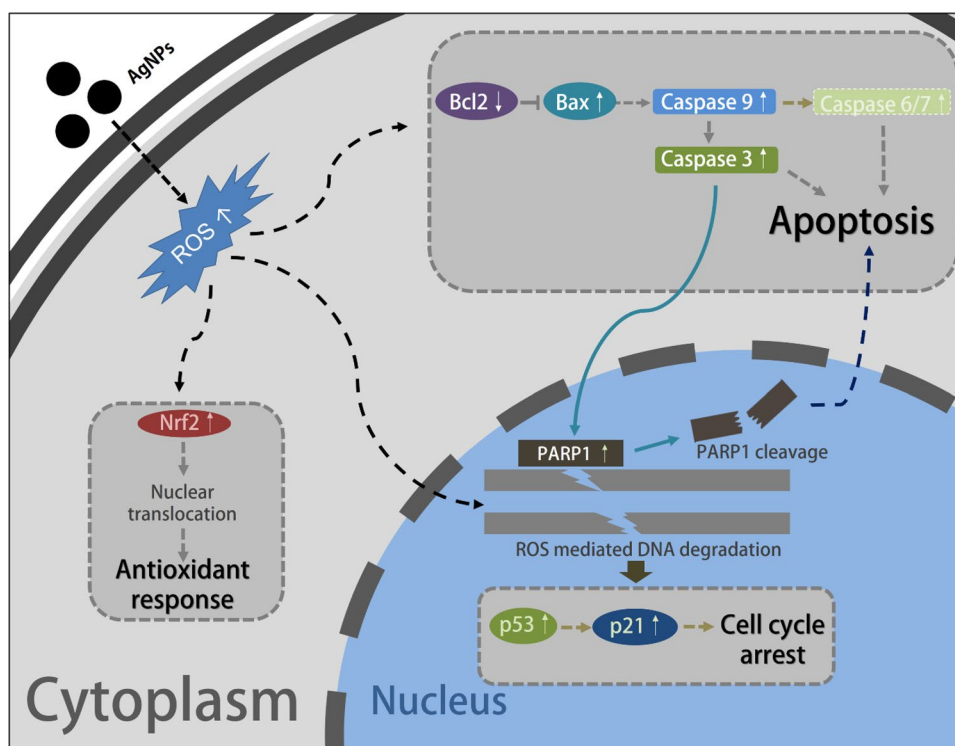
either Caspase-6 or -7 in MCF7 which is a Caspase-3-mutant [29]. After 24 h and 48 h, S_1 successfully induced Caspase-9 expression in both breast cancer cell lines. About 1.4 fold increase in Caspase-9 expression was observed following 48 h treatment. Caspase-3 was also found overexpressed in MDA-MB-231 after 24 h of treatments, where the maximum effect was observed following 48 h. At this time point, S_1 induced approximately 1.4 fold increase in its level as compared to the group without treatment. PARP1, which was found upregulated following ROS-mediated DNA damage in this experiment, was ultimately cleaved by activated effector caspases. The level of its cleaved form was found significantly high after 24 h of treatment which was detected highest after 48 h (2–2.4 fold increase). Presence of the cleaved PARP1 confirmed the caspase-mediated apoptosis in both cell lines as this is considered as a hallmark of apoptosis [26, 44]. Cumulatively, these findings clearly demonstrated that S_1 are effective against two different types of breast cancer cell lines and this cytotoxic property was attributed to cell cycle arrest and caspase-dependent intrinsic apoptosis pathway in absence of the extrinsic one.

Conclusions

This study evidences the successful synthesis of chitosan-functionalized silver nanoparticles at a size range of 13–22 nm. The cytotoxic potential of these synthesized

nanoparticles against human breast cancer cells is quite interesting. They reduced cancer cell survival in a dose-dependent manner and their effective cytotoxic dose is as low as around 6.5 ppb. At these concentrations, they are very less toxic to normal human peripheral blood lymphocytes which justifies it as a safer cytotoxic agent for cancer cells. The nanoparticles were found equally effective in both types of human breast cancer cells viz. hormone-responsive MCF7 and chemoresistant MDA-MB-231. They were unable to induce necrosis in cancer cells but strongly induced intrinsic apoptosis pathway following intracellular oxidative stress, DNA damage and cell cycle arrest. The effects of S_1 in both types of breast cancer cells are depicted in the Fig. 6. The significance of the study is based on the evidence that the synthesized silver nanoparticles, besides being biocompatible, are potent cytotoxic agents at very low concentrations against breast cancer, safe for normal cells too and promising for application in breast cancer therapy.

Compliance with ethical standards

References

1. Al-Otaibi WA, Alkhatib MH, Wali AN. Cytotoxicity and apoptosis enhancement in breast and cervical cancer cells upon coadministration of mitomycin C and essential oils in nanoemulsion formulations. Biomed Pharmacother. 2018;106:946–55.

2. Amaral I, Silva C, Correia-Branco A, Martel F. Effect of metformin on estrogen and progesterone receptor-positive (MCF-7) and triple-negative (MDA-MB-231) breast cancer cells. Biomed Pharmacother. 2018;102:94–101.

3. Azizi M, Ghourchian H, Yazdian F, Bagherifam S, Bekhradnia S, Nyström B. Anti-cancerous effect of albumin coated silver nanoparticles on MDA-MB 231 human breast cancer cell line. Sci Rep. 2017;7:1–18.

4. Bandyopadhyay A, Banerjee PP, Shaw P, Mondal MK, Das VK, Chowdhury P, et al. Cytotoxic and mutagenic effects of *Thuja occidentalis* mediated silver nanoparticles on human peripheral blood lymphocytes. Mater Focus. 2017;6:290–6.

5. Banerjee PP, Bandyopadhyay A, Harsha SN, Policegoudra RS, Bhattacharya S, Karak N, et al. *Mentha arvensis* (Linn.)-mediated green silver nanoparticles trigger caspase 9-dependent cell death in MCF7 and MDA-MB-231 cells. Breast Cancer Targets Ther. 2017;9:265–78.

6. Barua S, Banerjee PP, Sadhu A, Sengupta A, Chatterjee S, Sarkar S, et al. Silver nanoparticles as antibacterial and anticancer materials against human breast, cervical and oral cancer cells. J Nanosci Nanotechnol. 2017;17:968–76.

7. Bhattacharyya SS, Das J, Das S, Samadder A, Das D, De A, et al. Rapid green synthesis of silver nanoparticles from silver nitrate by a homeopathic mother tincture Phytolacca Decandra. Zhong Xi Yi Jie He Xue Bao. 2012;10:546–54.

8. Bhola PD, Letai A. Mitochondria—judges and executioners of cell death sentences. Mol Cell. 2016;61:695–704.

9. Bøyum A. Isolation of lymphocytes, granulocytes and macrophages. Scand J Immunol. 1976;5:9–15.

10. Castro-Aceituno V, Ahn S, Simu SY, Singh P, Mathiyalagan R, Lee HA, et al. Anticancer activity of silver nanoparticles from *Panax ginseng* fresh leaves in human cancer cells. Biomed Pharmacother. 2016;84:158–65.

11. Chaudhuri AR, Nussenzweig A. The multifaceted roles of PARP1 in DNA repair and chromatin remodelling. Nat Rev Mol Cell Biol. 2017;18:610–21.

12. Chen MC, Mi FL, Liao ZX, Hsiao CW, Sonaje K, Chung MF, et al. Recent advances in chitosan-based nanoparticles for oral delivery of macromolecules. Adv Drug Deliv Rev. 2013;65:865–79.

13. Comşa Ş, Cîmpean AM, Raica M. The story of MCF-7 breast cancer cell line: 40 years of experience in research. Anticancer Res. 2015;35:3147–54.

14. Das S, Das J, Samadder A, Bhattacharyya SS, Das D, Khuda-Bukhsh AR. Biosynthesized silver nanoparticles by ethanolic extracts of *Phytolacca decandra*, *Gelsemium sempervirens*, *Hydrastis canadensis* and *Thuja occidentalis* induce differential cytotoxicity through G2/M arrest in A375 cells. Colloids Surf B Biointerfaces. 2013;101:325–36.

15. Das S, Khuda-Bukhsh AR. PLGA-loaded nanomedicines in melanoma treatment: future prospect for efficient drug delivery. Indian J Med Res. 2016;144:181–93.

16. De Matteis V, Cascione M, Toma C, Leporatti S. Silver nanoparticles: synthetic routes, in vitro toxicity and theranostic applications for cancer disease. Nanomaterials. 2018;8:1–23.

17. Elinav E, Peer D. Harnessing nanomedicine for mucosal theranostics—a silver bullet at last? ACS Nano. 2013;7:2883–90.

18. Escoll M, Gargini R, Cuadrado A, Anton IM, Wandosell F. Mutant p53 oncogenic functions in cancer stem cells are regulated by WIP through YAP/TAZ. Oncogene. 2017;36:3515–27.

19. Franci G, Falanga A, Galdiero S, Palomba L, Rai M, Morelli G, et al. Silver nanoparticles as potential antibacterial agents. Molecules. 2015;20:8856–74.

20. Fulda S, Debatin KM. Extrinsic versus intrinsic apoptosis pathways in anticancer chemotherapy. Oncogene. 2006;25:4798–811.

21. Georgakilas AG, Martin OA, Bonner WM. p21: a two-faced genome guardian. Trends Mol Med. 2017;23:310–9.

22. Huang X, Qiao Y, Zhou Y, Ruan Z, Kong Y, Li G, et al. Ureaplasma spp. lipid-associated membrane proteins induce human monocyte U937 cell cycle arrest through p53-independent p21 pathway. Int J Med Microbiol. 2018;308:819–28.

23. Ingallina E, Sorrentino G, Bertolio R, Lisek K, Zannini A, Azzolin L, et al. Mechanical cues control mutant p53 stability through a mevalonate–RhoA axis. Nat Cell Biol. 2018;20:28–35.

24. Jin R, Cao YC, Hao E, Métraux GS, Schatz GC, Mirkin CA. Controlling anisotropic nanoparticle growth through plasmon excitation. Nature. 2003;425:487–90.

25. Karimian A, Ahmadi Y, Yousefi B. Multiple functions of p21 in cell cycle, apoptosis and transcriptional regulation after DNA damage. DNA Repair. 2016;42:63–71.

26. Kaufmann SH, Desnoyers S, Ottaviano Y, Davidson NE, Poirier GG. Specific proteolytic cleavage of poly(ADP-ribose) polymerase: an early marker of chemotherapy-induced apoptosis. Cancer Res. 1993;53:3976–85.

27. Khan Z, Singh T, Hussain JI, Obaid AY, Al-Thabaiti SA, El-Mossalamy EH. Starch-directed green synthesis, characterization and morphology of silver nanoparticles. Colloids Surf B Biointerfaces. 2013;102:578–84.

28. Kroll A, Pillukat MH, Hahn D, Schnekenburger J. Interference of engineered nanoparticles with in vitro toxicity assays. Arch Toxicol. 2012;86:1123–36.

29. Liang Y, Yan C, Schor NF. Apoptosis in the absence of caspase 3. Oncogene. 2001;20:6570–8.

30. Lowry OH, Rosebrough NJ, Farr AL, Randall RJ. Protein measurement with the Folin phenol reagent. J Biol Chem. 1951;193:265–75.

31. Ma Q. Role of Nrf2 in Oxidative Stress and Toxicity. Annu Rev Pharmacol Toxicol. 2013;53:401–26.

32. Mao BH, Chen ZY, Wang YJ, Yan SJ. Silver nanoparticles have lethal and sublethal adverse effects on development and longevity by inducing ROS-mediated stress responses. Sci Rep. 2018;8:1–16.

33. Mittal S, Pandey AK. Cerium oxide nanoparticles induced toxicity in human lung cells: role of ROS mediated DNA damage and apoptosis. Biomed Res Int. 2014;2014:1–14.

34. Mohammed M, Syeda J, Wasan K, Wasan E. An overview of chitosan nanoparticles and its application in non-parenteral drug delivery. Pharmaceutics. 2017;9:1–26.

35. Mukherjee S, Mitra I, Fouzder C, Mukherjee S, Ghosh S, Chatterji U, et al. Effect of Pt(II) complexes on cancer and normal cells compared to clinically used anticancer drugs: cell cycle analysis, apoptosis and DNA/BSA binding study. J Mol Liq. 2017;247:126–40.

36. Nguyen T, Nioi P, Pickett CB. The Nrf2-antioxidant response element signaling pathway and its activation by oxidative stress. J Biol Chem. 2009;284:13291–5.

37. Pan Y, Ye C, Tian Q, Yan S, Zeng X, Xiao C, et al. miR-145 suppresses the proliferation, invasion and migration of NSCLC cells by regulating the BAX/BCL-2 ratio and the caspase-3 cascade. Oncol Lett. 2018;15:4337–43.

38. Pascal JM. The comings and goings of PARP-1 in response to DNA damage. DNA Repair. 2018;71:177–82.

39. Reyes J, Chen JY, Stewart-Ornstein J, Karhohs KW, Mock CS, Lahav G. Fluctuations in p53 signaling allow escape from cell-cycle arrest. Mol Cell. 2018;71:581–91.

40. Romanov VS, Rudolph KL. p21 shapes cancer evolution. Nat Cell Biol. 2016;18:722–4.

41. Roy B, Mukherjee S, Mukherjee N, Chowdhury P, Babu SP. Design and green synthesis of polymer inspired nanoparticles for the evaluation of their antimicrobial and antifilarial efficiency. RSC Adv. 2014;4:34487–99.

42. Satchell P, Gutmann J, Witherspoon D. Apoptosis: an introduction for the endodontist. Int Endod J. 2003;36:237–45.

43. Shalini S, Dorstyn L, Dawar S, Kumar S. Old, new and emerging functions of caspases. Cell Death Differ. 2015;22:526–39.

44. Wang H, Zhang G. Endoplasmic reticulum stress-mediated autophagy protects against β, β-dimethylacrylshikonin-induced apoptosis in lung adenocarcinoma cells. Cancer Sci. 2018;109:1889–901.

45. Yuan YG, Zhang S, Hwang JY, Kong IK. Silver nanoparticles potentiates cytotoxicity and apoptotic potential of camptothecin in human cervical cancer cells. Oxid Med Cell Longev. 2018;2018:1–21.

46. Zhang XF, Liu ZG, Shen W, Gurunathan S. Silver nanoparticles: synthesis, characterization, properties, applications, and therapeutic approaches. Int J Mol Sci. 2016;17:1–34.

47. Zhu L, Han MB, Gao Y, Wang H, Dai L, Wen Y, et al. Curcumin triggers apoptosis via upregulation of Bax/Bcl-2 ratio and caspase activation in SW872 human adipocytes. Mol Med Rep. 2015;12:1151–6.